



Time-Accurate Coupling of Three-Degree-of-Freedom Parachute System with Navier–Stokes Equations

G. P. Guruswamy*

NASA Ames Research Center, Moffett Field, California 94035

DOI: 10.2514/1.A33835

A parachute with payload is modeled as a three-degree-of-freedom system suitable for time-accurate coupling with the Navier–Stokes flow equations. The coupled equations of motion are formulated following an instantaneous Lagrangian–Eulerian approach, and solved using Newmark’s time-integration method. Flow solutions are computed by solving the Reynolds-averaged Navier–Stokes equations with structured overset grids. A sensitivity analysis is used to check the adequacy of grid and time-step requirements. The time-accurate coupling procedure is validated by comparing the results with a frequency-domain approach. The results are demonstrated for a real parachute system, including a comparison with the results based on the linear theory. Possible instabilities, such as divergence of inclination angle and flutter associated with fluctuating drag force, are predicted. The present work advances the fidelity of analysis procedures beyond those in current use based on loose coupling with the Navier–Stokes equations.

Nomenclature

C_D, C_Z	=	drag and side-force coefficients
D	=	diameter of the base of a canopy, m
E	=	modulus of elasticity of a canopy fabric, Pa
g	=	acceleration due to gravity, m/s ²
k_d	=	reduced frequency, $\omega D/U$
L	=	distance between the mass centers of a canopy and store, m
M	=	Mach number
m_a	=	aerodynamic mass around a canopy, kg
m_c, m_s	=	canopy and store mass, kg
q	=	dynamic pressure, $0.5\rho U^2$, kg/m ²
Re_D	=	Reynolds number based on D
t	=	time, s
U	=	speed, m/s
θ	=	inclination or coning angle, deg
ν	=	Poisson’s ratio
ρ	=	density of air, kg/m ³
ω	=	oscillatory frequencies, rad/s
∞	=	freestream condition

I. Introduction

THE use of parachutes is an integral component of descent systems. The new NASA spacecraft that will carry a crew exploration vehicle (CEV), known as Orion, will accommodate up to six astronauts and will use parachutes during its descent stage. A critical component of the Orion design is the parachute deceleration system, which is required to ensure safe landing of the capsule [1]. For a safe landing on Mars, supersonic parachutes are used [2].

Parachutes, of course, have been successfully used in aerospace programs since the Apollo missions. However, as stated in [3], a major difficulty in the design and development of these deceleration systems is the lack of adequate analytical methods to properly predict dynamic behavior, including loads and stresses on parachute systems. These systems involve moving components in flows dominated by vortices and their complex interactions, and a strong nonlinear coupling that occurs between the flowfield and structural elements associated with large movements [3].

The stability of the parachute system is critical for the safe and accurate landing of payloads, particularly when the crew is involved. Complex flows coupled with multibody motions, including flexible (canopy) and rigid (capsule), are a few of the elements involved in determining the system’s stability. Figure 1 shows an unstable parachute system after a successful deployment. Significant coupling between the flow and canopy fabric occurred after full deployment, which might have led to a system failure.[†]

The accurate modeling of flows around a parachute system requires a solution of the unsteady Navier–Stokes equations through the use of computational fluid dynamics (CFD), which can efficiently model moving grids, including bodies with motion relative to each other. The use of such a tool is critical, because the CEV capsule will have more payload than the Apollo capsule, and may be required to land on the ground [1].

Since the Apollo program, computational methods for both fluids and structures have advanced significantly. However, the design of the parachute system for the Orion capsule still uses the linear aerodynamic theory available in NASTRAN, a finite element analysis program developed in the late 1960s. The multibody dynamics is modeled using the ADAMS module [4].

Applications of higher-fidelity models for parachutes have been recently applied. The work in [5] presents computations on a flexible isolated canopy with a capsule using the Euler equations, and included the validation of pressures with the experiment. Takizawa et al. [6] present a finite element approach to solve incompressible flows over flexible canopy clusters, but did not include a capsule or any validation. Recently, Reynolds-averaged Navier–Stokes (RANS)-equation-based computations have been presented for a cluster of rigid canopies with a capsule [7] using the overset-grid-based RANS solver, OVERFLOW [8], and included validations with the experiment. To date, the fluids/structures-interface efforts for parachutes using CFD codes are based on quasi-steady (also known as loose) coupling [9].

A survey of related literature within the scope of this work reveals that the aeroelastic data needed to validate CFD for parachute systems are seldom available in the public domain. Most of the data available are in the form of global stability derivatives for a complete system, without details, such as surface pressures. The majority of previously published data using CFD have relied on the argument of its own self-consistent calculations and models [6]. In this paper, the compressible/incompressible CFD code OVERFLOW, which is well validated with third-party data for steady and unsteady flows over complex configurations, is selected for parachute-system analysis. OVERFLOW has also been validated for flexible configurations [10], and has a robust ability to model moving components [11]. Additional validation is established by comparing the results between

Received 16 December 2016; revision received 8 May 2017; accepted for publication 11 May 2017; published online 18 July 2017. This material is declared a work of the U.S. Government and is not subject to copyright protection in the United States. All requests for copying and permission to reprint should be submitted to CCC at www.copyright.com; employ the ISSN 0022-4650 (print) or 1533-6794 (online) to initiate your request. See also AIAA Rights and Permissions www.aiaa.org/randp.

*Aerospace Engineer, Computational Physics Branch. Associate Fellow AIAA.

[†]www.space.com/29602-nasa-flying-saucer-supersonicparachute-fails.html.

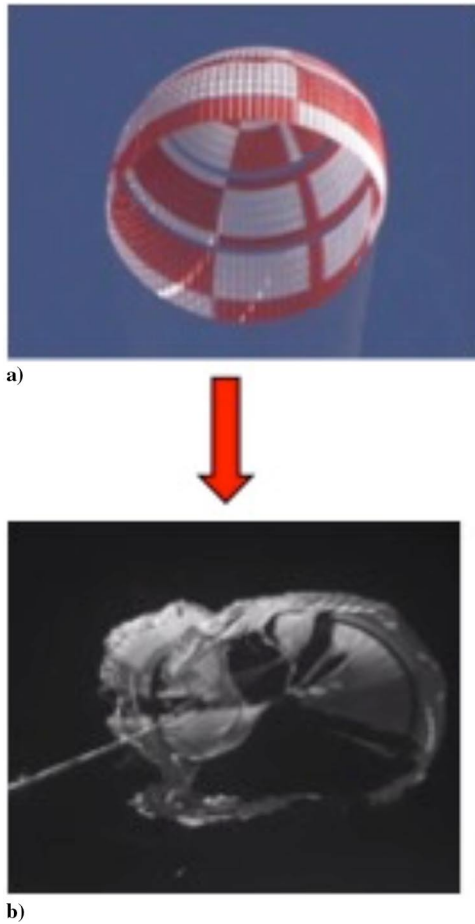


Fig. 1 Unstable parachute after successful deployment: a) deployment and b) unstable.

time-response and frequency-domain approaches along with a comparison with the linear theory.

II. Three-Degree-of-Freedom System

Pendulum motion in two dimensions is a primary mode of oscillation for a parachute with a payload [12]. Figure 2 shows a parachute with a capsule as a payload. It is assumed that the pendulum motion occurs in the x - z plane about the y axis. The masses in consideration in this simulation are payload mass m_p , canopy mass m_c , and the aerodynamic added mass within a canopy m_a . The basic model of a two-dimensional system can be represented as a three-degree-of-freedom (3-DOF) system about the center of total mass involving rotation θ , and translations along the x axis and z axis. The following assumptions are made:

- 1) The mass m_a depends only on the canopy.
- 2) The centers of m_c and m_a are coincident.
- 3) The masses m_c and m_p are at a fixed distance apart of L .
- 4) The centers of forces on a canopy and its mass are coincident.
- 5) The aerodynamic force on a payload is small compared to that on a canopy.

The equations of motion governing the system are written as

$$\frac{d^2\theta}{dt^2} + \left[\frac{g}{L(1 + m_c m_a^{-1})} \right] \theta - \frac{F_N}{L(m_a + m_c)} = 0 \quad (1)$$

$$m_s \frac{d^2x}{dt^2} - m_t g + F_A \cos \theta - F_N \sin \theta = 0 \quad (2)$$

$$m_s \frac{d^2z}{dt^2} + F_A \sin \theta + F_N \cos \theta = 0 \quad (3)$$

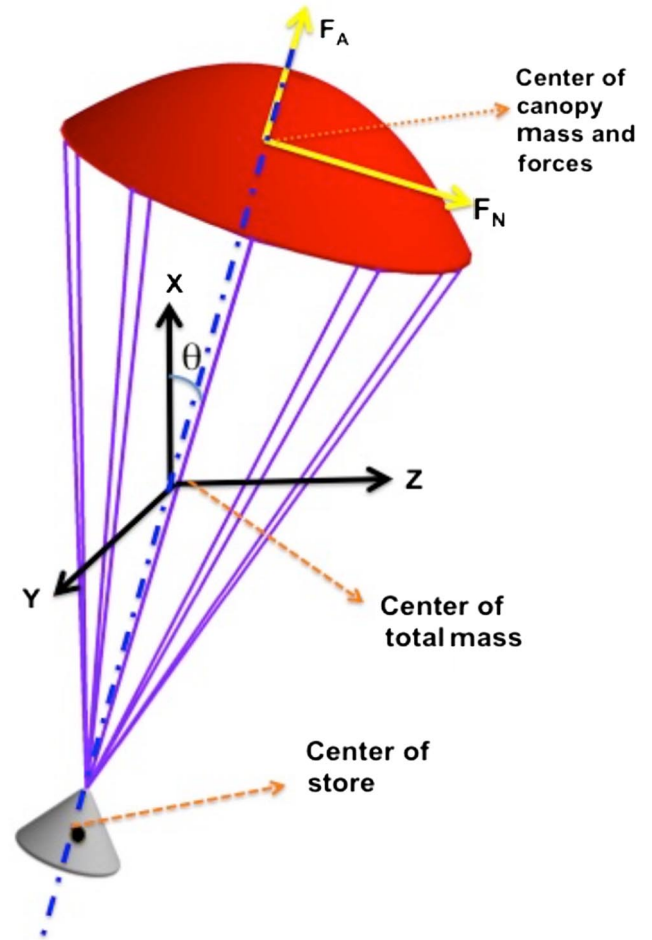


Fig. 2 Three-degree-of-freedom parachute model.

in which the total structural mass is $m_s = (m_c + m_p)$, the total system mass is $m_t = (m_c + m_p + m_a)$, g is the acceleration due to gravity, and L is the distance between the mass centers of the canopy and payload.

In this effort, the flexibility of the canopy is represented by breathing modes (shrinking and expanding along the x axis that result in changes along the circumference) and squeezing modes (shrinking and expanding in the z - x plane that result in changes only in circumferential direction). Oscillations in breathing and squeezing modes are predominant during descent and pendulum-type motions, respectively.

The flexibility of the canopy is modeled based on the simplified equations given in table 29 of [13] for thin shells subjected to external pressure. The rate of change in the diameter ΔD of the canopy base is given by

$$\frac{\Delta D}{D} = \frac{q c_d D (1 - \nu)}{4Et} \quad (4)$$

in which ν is Poisson's ratio, E is the modulus of elasticity, and t is the thickness of the canopy material. The dynamic pressure is represented by q , whereas c_d is the drag coefficient. The diameters along the axis are changed with the same proportion as the change in the diameter of the base. The change in the height of the canopy is computed assuming that the total volume of the canopy remains constant.

Equation (1) is solved using Newmark's time-integration method in association with the instantaneous Lagrangian-Eulerian approach (known as arbitrary Lagrangian-Eulerian) [14], with the aerodynamic data F_A and F_N computed by solving RANS equations [15]. For this work, the RANS equations are numerically solved using the diagonal form of the Beam-Warming central-difference algorithm [16], along with the one-equation Spalart-Allmaras turbulence model [17].

Using the computed coning angle from Eq. (1), Eqs. (2) and (3) are solved to compute the trajectory motions in the x and z directions.

III. Validation of Time Integration

Grids for the canopy and capsule are taken from the previous paper by the author [7]. The hemispherical canopy shown in Fig. 2 has a spill hole of 5% diameter. As shown in Fig. 3, the canopy is modeled with a body-fitted near-body grid with a C–O topology (C along the radial direction and O in the circumferential direction). The number of grid points along the radial direction for the canopy is 349, and the numbers of points in the circumferential and normal directions are 61 and 74, respectively. The grid has a normal spacing of $0.000025D$ with a surface stretching factor of 1.125, which yields a y^+ value (one grid point away from the surface) that varies between 0.959 and 1.14, and is considered adequate to resolve flows at the surface. The spill hole is modeled using a cylindrical grid with 11 radial points, 147 axial points, and 61 circumferential points. The direction of the flow is assumed to be in the positive direction of the x axis.

The spherical grid for the capsule is modeled based on the Apollo command module as in [8], and has 115 circumferential, 61 radial, and 60 normal grid points. The cluster is embedded in the Cartesian outer grid with the size of $201 \times 138 \times 138$, resulting in a total grid size of about 6 million points. The outer boundaries are located at 15 diameters from the vertex of the stationary canopy.

Computations for validation are performed for a freestream Mach number $M_\infty = 0.3$. The Reynolds number based on the canopy diameter Re_D is 2×10^6 . Figure 4 shows the steady-state field Mach number and surface-pressure distributions when the canopy is stationary.

First, computations are made for pendulum-type oscillations. To verify the time-integration results, responses are obtained by forcing the system to oscillate in sinusoidal motion without allowing the canopy to deform. Equation (1) is written in a simpler form by introducing the damping parameter A_1 :

$$\frac{d^2\theta}{dt^2} + A_1\dot{\theta} + A_2\theta = A_3c_z \cos(\theta) \quad (5)$$

Figure 5 shows that the side force c_z response leads the motion by 8 deg under forced sinusoidal motion. Based on this phase angle,

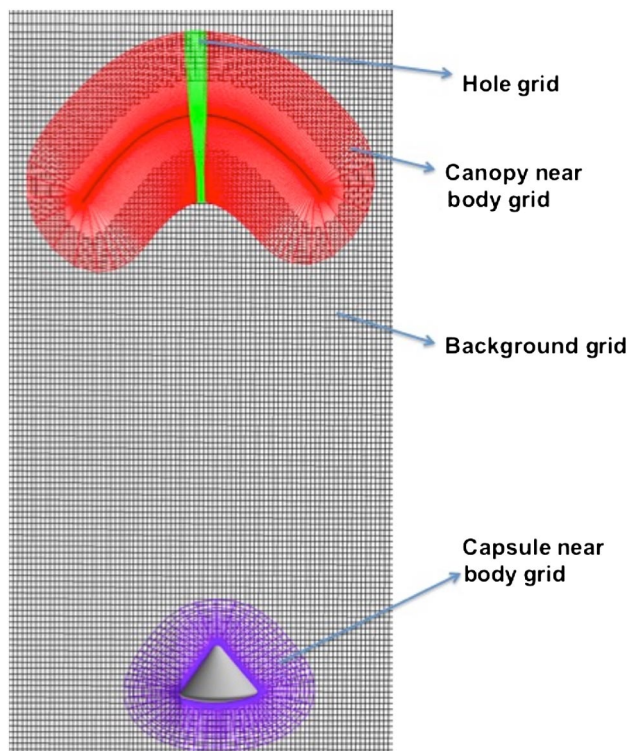


Fig. 3 Grid topology.

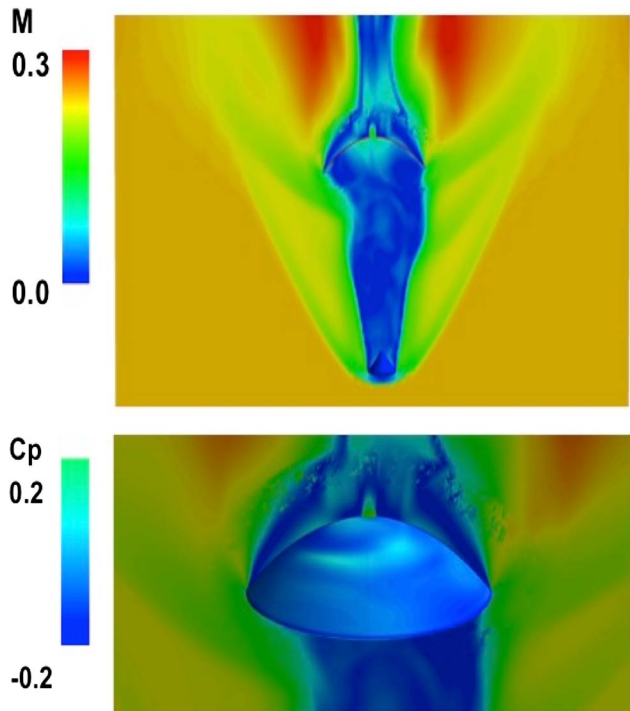


Fig. 4 Field Mach-number contours and canopy surface pressures at $M = 0.30$.

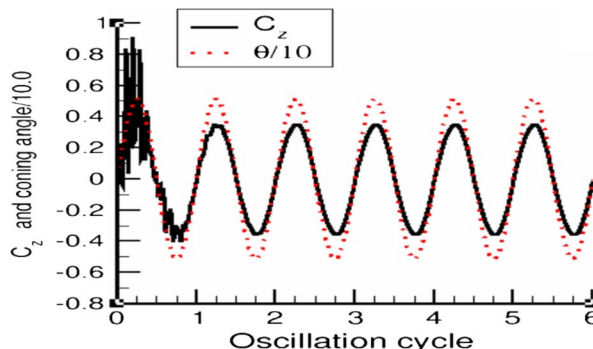


Fig. 5 Force response due to forced sinusoidal motion.

coefficients A_1 and A_2 are found by setting $A_3 = 1.0$ for a neutral response, and equating in-phase and out-of-phase quantities of Eq. (5). Time integration using A_1 and A_2 results in an almost neutral response, as shown in Fig. 6. Reduction of structural damping A_1 by 10% results, as one expects, in a diverging response shown in Fig. 6. Also, as expected, an increase of A_1 by 10% resulted in a converging response (not shown in Fig. 6). The neutral response obtained using the coefficients from the forced-response analysis shown in Fig. 5 and the diverging/converging responses obtained with variations of A_1

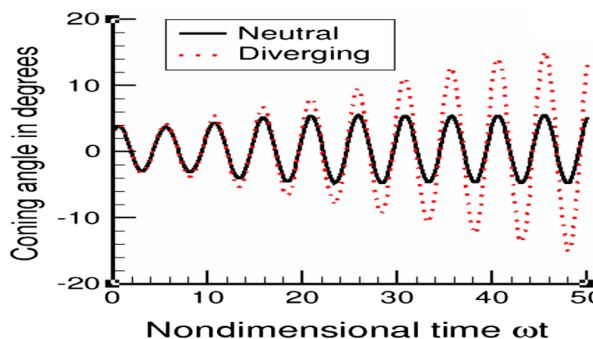


Fig. 6 Neutral and diverging responses in pendulum motion.

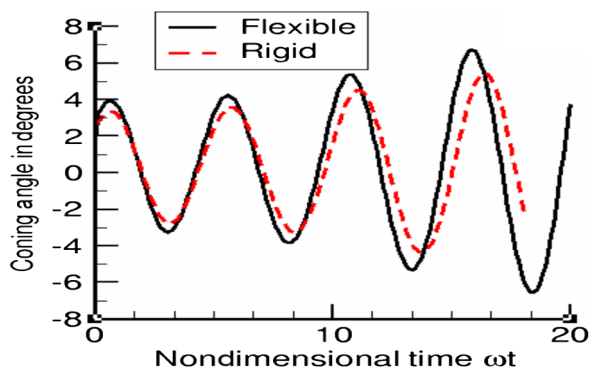


Fig. 7 Effect of flexibility of aeroelastic response.

verify the implementation of the time-integration method using RANS equations.

Figure 7 shows the effect of flexibility on aeroelastic response using Eq. (4). The rigid model yields a more conservative response than the flexible model.

IV. Demonstration for a Typical Canopy–Capsule System

The typical canopy–payload system similar to that described in [12] is selected for demonstration of results for a realistic configuration. The values of the physical parameters of the configuration are as follows: base diameter of the canopy $D = 4.4$ m, length between the mass centers of the canopy and store $L = 8.4$ m, mass of the canopy $m_c = 7$ kg, mass of the payload $m_p = 91$ kg, aerodynamic mass $m_a = 124$ kg based on Henrich formula [12], modulus of elasticity of the canopy fabric $E = 90$ MPa, and Poisson's ratio $\nu = 0.20$.

Two flight conditions with initial Mach numbers 0.43 and 2.0 listed in [18] are considered for demonstration. The nondimensional time-step size ($\Delta t U/D$) and number of Newton iterations are determined by numerical experiments. It is found that 10 Newton iterations are adequate for a stable solution. Based on the convergence history shown in Fig. 8, the time step needed for accuracy that corresponds to the system oscillating at 1 Hz with 480 steps per cycle is 0.0131.

The first computations are made for the subsonic case deployment starting at $M_\infty = 0.43$. As given in [18], the dynamic pressure $q = 73.5$ Pa and the deployment velocity is 103.6 m/s. To begin, steady computations are made for a rigid case with a mean inclination angle of $\theta = 0.0$ deg until the residual dropped about three orders of magnitude. Then, aeroelastic computations are started to integrate equations of motion (1). The following numerical-integration procedure is used.

Starting from the converged steady-state solution, loads are computed for the first time step. Using these loads, Eq. (1) is integrated in a module outside the CFD code using Newmark's time-integration method, as described in [14]. Integration is started with an initial

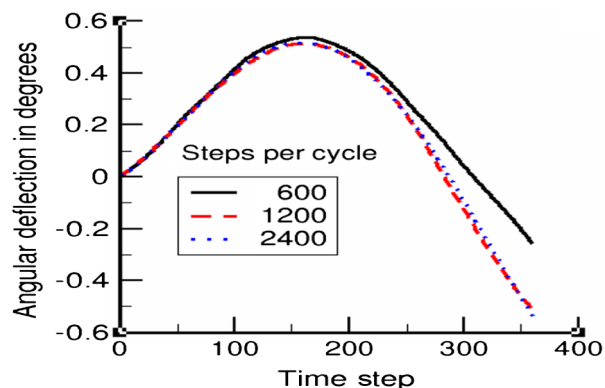


Fig. 8 Convergence of θ with respect to decreasing time-step size.

nondimensional velocity of 0.01. Using the new θ computed, the Mach number and position of the system for the next step are computed, solving Eqs. (2) and (3). The modal deformations are computed using Eq. (4). Updated values are used to determine the next position accounting for time metrics. This process is repeated until all required responses are obtained.

Figure 9 shows the comparison of inclination angles between the present computations and the simplified linear theory [12] for the first cycle. The period of the first cycle of θ from Fig. 9 is 5.2 s compared to 5.62 s based on the linear theory [12]. The peak amplitudes of the present results are smaller than that given by the linear theory. The linear theory without viscous and nonlinear terms may be overpredicting responses. The close comparison further validates the present time-integration approach with the Navier–Stokes equations.

Figure 10 shows the plots of inclination angle and drag responses along with descent Mach number. The Mach number decreases almost linearly, whereas the drag force decreases monotonically. The inclination angle shows oscillatory response with small amplitude due to initial disturbance.

The next computations are made at the supersonic Mach number 2.0. Based on [18], the dynamic pressure q and speed U are 753 Pa and 451 m/s, respectively. Computations without structural damping are started from a converged steady-state solution with an initial θ of 0.01 using a nondimensional time step of 0.0131 based on the results shown in Fig. 8. Figure 11 shows the response results for the first 2.5 s during which the Mach number decreases from 2.0 to 1.6. The inclination angle shows a diverging trend, and drag responses are oscillatory with slightly decreasing amplitude. The magnitude of amplitude decreases from 7 to 3%.

Computations are repeated with Raleigh-type structural damping of a value equal to 90% of the stiffness coefficient of θ in Eq. (1), and the results are plotted in Fig. 12. The addition of structural damping

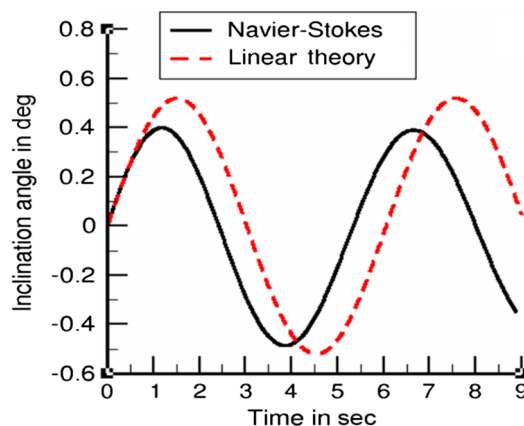


Fig. 9 Comparison between the linear theory and present computations.

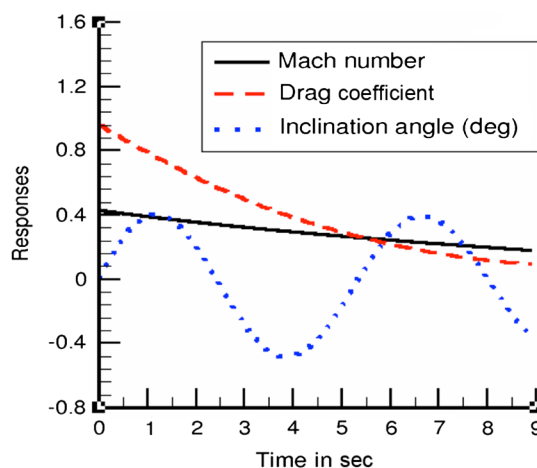


Fig. 10 Responses for case with deployment $M_\infty = 0.43$.

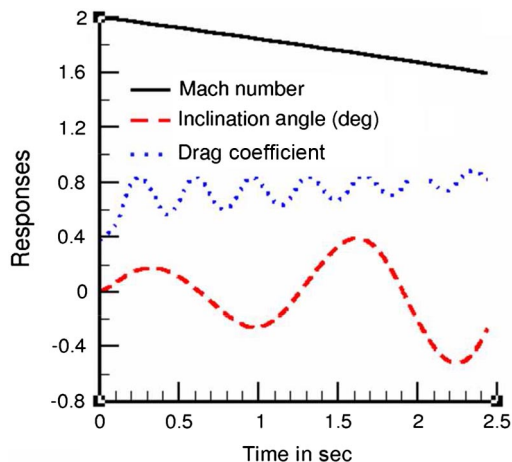


Fig. 11 Responses during descent from $M_\infty = 2.0$.

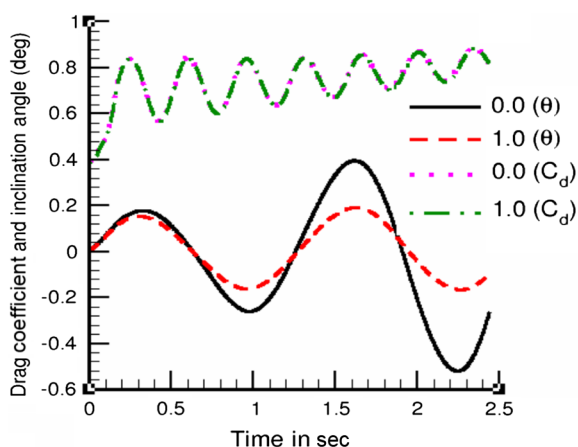


Fig. 12 Effect of structural damping on responses.

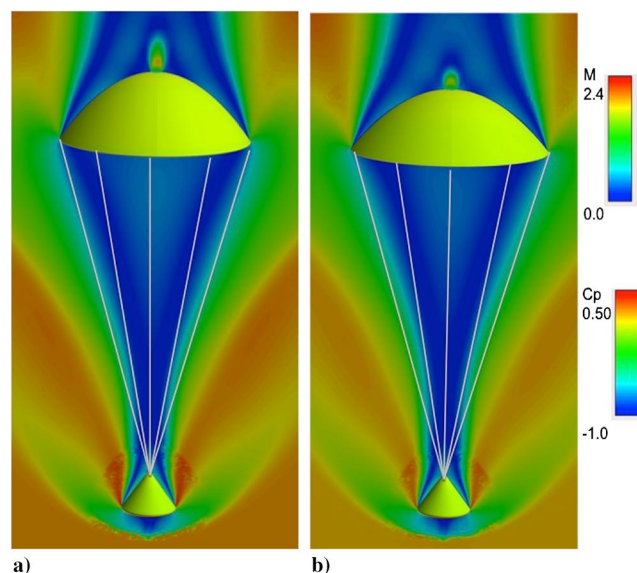


Fig. 13 Snapshots from when the canopy is at a) start and b) at about 1.5 s.

makes the response of the inclination angle more stable, but does not have observable effects on drag coefficient. However, the amplitude of the drag coefficient reduces in time as in the undamped case.

Figure 13 shows the snapshots of field Mach number and surface c_p at the start position and the peak bulged position around $t = 1.56$ s. Mach numbers below the canopy for the peak position

have a larger subsonic region below the canopy surface than at the start position. Flow around the hole has a lesser supersonic region for $t = 1.56$ s. The bulging and shrinking of the canopy are due to fluctuations of c_d , as shown in Fig. 11.

V. Conclusions

To date, stability analyses for parachute systems are often performed by others using linear aerodynamic theories. The use of advanced flow models, such as those based on the Navier–Stokes equations, is limited to quasi-steady coupling. In this study, a Reynolds-averaged Navier–Stokes (RANS)-equation-based high-fidelity procedure valid for both compressible and incompressible flows is time accurately coupled with a 3-three-degree-of-freedom parachute–payload system. The flexibility of the canopy is represented in the modal form. The coupling procedure accommodates for trajectory motions, and the time-accurate coupling procedure is validated with a frequency-domain approach. Demonstration results are shown for stable and unstable responses, including the effect of flexibility.

The results are computed for a system with realistic physical parameters. The frequency and amplitude of responses vary from those based on the linear theory, but show the same trends. Computations for both subsonic and supersonic ranges show that the system is unstable without structural damping. Stabilizing the system by adding structural damping is demonstrated. The onset of possible flutter at supersonic regime is predicted by the present time-integration method. Such predictions are not possible by loose coupling used elsewhere. The present work provides a high-fidelity-based analysis procedure for designing parachutes.

Further developments are needed in this area by extending the time integration with the use of three-dimensional trajectory equations. The use of the finite element modeling of structures in place of modes can facilitate the direct computation of stresses during the trajectory analysis. For including more flow details, the RANS equations need to be replaced with the direct Navier–Stokes equations, taking advantage of rapidly growing computer resources. The present effort is accomplished by extensively modifying the existing popular computational fluid dynamics (CFD) code that was primarily designed for rigid configurations. A more general-purpose, modular, and robust fluid/structure-interaction capability is needed for CFD codes to accommodate full trajectory equations.

Acknowledgments

This work was partly supported under the technology development activities of the NASA Advanced Supercomputing (NAS) Division. The author would like to thank Nagi Mansour, Computational Physics branch Chief at the NAS Division for valuable suggestions during this effort.

References

- [1] Marshall, P., and Norris, S. D., "Orion Program Status," *AIAA Space 2013 Conference and Exhibition*, AIAA Paper 2013-5476, Sept. 2013.
- [2] Anon., "NASA's LDSD Project Completes Second Experimental Test Flight," NASA Jet Propulsion Lab., June 2015, <http://www.jpl.nasa.gov/news/news.php?release=2015-197> [retrieved 14 June 2017].
- [3] Knacke, T. W., "The Apollo Parachute Landing System," *AIAA Second Aerodynamic Deceleration Conference*, El Centro, CA, Sept. 1968.
- [4] Moore, J. W., and Romero, L. M., "An Airborne Parachute Compartment Test Bed for the Orion Parachute Test Program," *AIAA Aerodynamic Decelerator Systems (ADS) Conference*, AIAA Paper 2013-1289, March 2013.
- [5] Guruswamy, G. P., "Euler/Navier–Stokes Based Unsteady Aerodynamics and Aeroelasticity of a Capsule Landing System," *48th AIAA Structural Dynamics Conference*, AIAA Paper 2007-2063, April 2007.
- [6] Takizawa, K., Wright, S., Moorman, C., and Tezduyar, T. E., "Fluid–Structures Interaction Modeling of Parachute Clusters," *International Journal for Numerical Methods in Fluids*, Vol. 65, Nos. 1–3, May 2011, pp. 286–307. doi:10.1002/flid.v65.1/3
- [7] Guruswamy, G. P., "Fast Database Generation for Parachute Cluster Design Using Navier–Stokes Equations on Supercomputers," *Journal of*

- Spacecraft and Rockets*, Vol. 52, No. 6, Nov.–Dec. 2015, pp. 1542–1550. doi:10.2514/1.A33360
- [8] Nichols, R. H., Tramel, R. W., and Buning, P. G., “Solver and Turbulence Model Upgrades to OVERFLOW2 for Unsteady and High-Speed Applications,” *AIAA 36th Fluid Dynamics Conference*, AIAA Paper 2006-2824, June 2006.
- [9] Karagiozis, K., Kamakoti, R., Cirak, F., and Pantano, C., “A Computational Study of Supersonic Disk-Gap-Band Parachutes Using Large-Eddy Simulation Coupled with Structural Membrane,” *Journal of Fluids and Structures*, Vol. 27, No. 2, 2011, pp. 175–192. doi:10.1016/j.jfluidstructs.2010.11.007
- [10] Guruswamy, G. P., “Computational-Fluid-Dynamics- and Computational-Structural-Dynamics-Based Time-Accurate Aeroelasticity of Helicopter Blades,” *Journal of Aircraft*, Vol. 47, No. 3, May–June 2010, pp. 858–863. doi:10.2514/1.45744
- [11] Flora, T. J., and Johnson, R., “Comparison of Experiments and OVERFLOW Modeling of Store Release from a Cavity at Mach 3,” *Overset Symposium*, June 2017, 2012.oversetgridssymposium.org/index.php [retrieved 14 June 2017].
- [12] Hume, R. G., “A Two-Dimensional Mathematical Model of a Parachute in Steady Descent,” Aeronautical Research Council CP No. 1260, Feb. 1973.
- [13] Roark, R. J., and Young, W. C., *Formulas for Stress and Strain*, 5th ed., McGraw–Hill, New York, 1975, pp. 445–451.
- [14] Guruswamy, G. P., “Time-Accurate Aeroelastic Computations of a Full Helicopter Model Using the Navier–Stokes Equations,” *International Journal of Aerospace Innovations*, Vol. 5, Nos. 3–4, Dec. 2013, pp. 73–82. doi:10.1260/1757-2258.5.3-4.73
- [15] Peyret, R., and Viviand, H., “Computation of Viscous Compressible Flows Based on Navier–Stokes Equations,” AGARD AG-212, 1975.
- [16] Beam, R. M., and Warming, R. F., “An Implicit Factored Scheme for Compressible Navier–Stokes Equations,” *AIAA Journal*, Vol. 16, No. 4, 1978, pp. 393–402. doi:10.2514/3.60901
- [17] Spalart, P. R., “Direct Simulation of a Turbulent Boundary Layer,” *Journal of Fluid Mechanics*, Vol. 187, Feb. 1988, pp. 61–98. doi:10.1017/S0022112088000345
- [18] Lingard, J. S., Darley, M. G., and Underwood, J. C., “Simulation of Mars Supersonic Parachute Performance and Dynamics,” *19th AIAA Aerodynamic Decelerator Systems Technology Conference and Seminar*, AIAA Paper 2007-2507, May 2007.

R. M. Cummings
Associate Editor